Torque Controlled Locomotion of a Biped Robot with Link Flexibility

Nahuel A Villa, Pierre Fernbach, Nicolas Mansard, Olivier Stasse

Addressing Flexibility in Biped Locomotion with Robust Control and Closed-loop Model-Predictive Control

Nahuel A. Villa[1], Pierre Fernbach[2], Nicolas Mansard[1,3], Olivier Stasse[1,3]

***Abstract*— While the last two years have seen the rise of many quadruped robots with excellent locomotion capabilities, biped robots are still limited, as they are evolving in a stability zone of reduced size. When transferring a locomotion controller from simulation to reality, modeling errors are then difficult to compensate with feedback only. This consequently imposes drastic constraints on the hardware design. In this paper, we propose to consider the simulation-to-reality gap by designing a robust locomotion controller. The robustness is obtained by a quantitative analysis of uncertainties, leading to bounds on its effects. As these bounds are compatible with the robot constraints, we propose a robust controller able to produce dynamic walking gaits. Feedback is obtained through the robust controller, acting as a balance stabilizer, and through a closed-loop model-predictive controller modeling the centroidal dynamics. We apply the proposed scheme to control the locomotion of the humanoid robot Talos, whose hip is mechanically flexible by design. We demonstrate in simulation the importance of the robustness to handle this situation and show its application in various scenarios in stairs and subject to important disturbances.**

I. INTRODUCTION

The stability of legged robots over their feet relies only on ground contact forces, which are strongly restricted. In fact, we can observe that less restrictive platforms, such as quadruped robots, have reached a maturity level that allows prototypes to manage properly the locomotion in many diverse scenarios [1], offering even commercial applications for the industry [2]. Bipeds, on the other hand, still require a much higher level of accuracy in sensors, actuators and models, as well as less dynamic movements to keep uncertainties under control with feasible contact forces.

We cannot change the physical limitation of forces, but based on reachability and set invariance (robust control), we found precise bounds for the set of stabilizable uncertainties [3]. These bounds provide a principled approach to set safety margins, to decide optimal feedback gains, and are central in the implementation of tube-based MPC [4]. In this article, we propose the implementation of a full controller for the locomotion of biped robots with explicit care of disturbances. We design a centroidal stabilizer based on state feedback that minimizes deviations from the desired motion, and we generate on-line such desired motion tacking actively into account the actual state of the robot with a closed-loop form of MPC [5].

*This work was supported by the cooperation agreement ROB4FAM.

1 Gepetto Team, LAAS-CNRS, Université de Toulouse, France.
2 TOWARD, Toulouse, France.
3 Artificial and Natural Intelligence Toulouse Institute, France.
e-mails: first_name.last_name@laas.fr, pierre.fernbach@toward.fr

In particular, we deploy this controller on the robot Talos: Talos is an anthropomorphic robot equipped with powerful actuators and precise sensors in a strong structure [6]. Nevertheless, this robot is manufactured with certain flexibility in the hip link that affects meaningfully its locomotion.

Flexible or compliant material is not uncommon in humanoid robotics. Robots such as Walkman [7] allows to directly tune the actuators' stiffness. Such actuators are notoriously known to be difficult to control and thus are the subject of advanced control strategies [8]. In our case, however, the deflection is not directly measurable as it is produced in the hip link, and we cannot modify it. Another example of humanoid robot with compliant material is HRP-2. It includes a bush rubber in the ankle in order to smooth impacts. In [9], a two stages controller using torque control is proposed in order to compensate for the deflection introduced by the compliant material. It assumes that the planned motion is generating no torque on the material in the best case, or that the deformation is known in advance. An indirect measure of deformations would be possible by using torque measurements of each joint and the robot dynamics. But the noise in torque sensors requires filtering, which introduces important delays. Unfortunately, previous experiences with such a technique carried out in the robot gave poor performances.

In this article, we propose to address this issue with a local compensation of deflections inspired on the standard methods described in [10]: We make an approximate estimation of hip deflections based on the commanded torques, and we combine them with the joint encoder measures to obtain an equivalent rigid robot configuration. We show in simulations that, as a result of this compensation, the remaining disturbances are close to those found with a non-flexible robot, which can be properly managed by the stabilizer.

The robot model for locomotion and its flexibility is discussed in Section II. Our centroidal controller is composed by a stabilizer, described in Section III, and predictive control, described in Section IV. The resulting locomotion instructions are taken by the whole-body controller, as explained in Section V, to compute the required joint torques. Based on such torques, Section VI proposes a method to compensate locally for hip deflections. The resulting full controller is tested in simulations by Section VII, and Section VIII summarizes the main conclusions of this article.

II. MODELING

A. Whole-body model and notations

Walking robots are normally represented as a kinematic chain of n joints connecting $n+1$ links, in which no link is attached to the inertial world frame [11]. The robot configuration $q = [q_w^\top \quad q_j^\top]^\top$ can be described by the position and orientation of the base link (robot waist) $q_w \in SE(3)$, and the posture given by all joint angles $q_j \in \mathbb{R}^n$.

Joint motors produce the torques $\tau_a \in \mathbb{R}^n$, required for the robot motion, following the dynamics:

$$\begin{bmatrix} M_u \\ M_a \end{bmatrix} \ddot{q} + \begin{bmatrix} h_u \\ h_a \end{bmatrix} = \begin{bmatrix} 0 \\ \tau_a \end{bmatrix} + \sum_k \begin{bmatrix} J_{u,k}^\top \\ J_{a,k}^\top \end{bmatrix} f_k, \tag{1}$$

where $M = \begin{bmatrix} M_u^\top & M_a^\top \end{bmatrix}^\top \in \mathbb{R}^{n+6 \times n+6}$ is the generalized inertia matrix, $h = \begin{bmatrix} h_u^\top & h_a^\top \end{bmatrix}^\top \in \mathbb{R}^{n+6}$ stands for Coriolis, centrifugal and gravity forces, and for each $_k$, $f_k \in \mathbb{R}^3$ is a force exerted by the environment on the point asociated to the Jacobian matrix $J_k^\top = \begin{bmatrix} J_{u,k} & J_{a,k} \end{bmatrix}^\top \in \mathbb{R}^{n+6 \times 3}$.

Joint angles must lie on collision-free ranges, and joint torques are limited by the employed motors and materials:

$$q_j^{min} \leq q_j \leq q_j^{max}, \tag{2}$$
$$\tau_a^{min} \leq \tau_a \leq \tau_a^{max}, \tag{3}$$

where the inequalities with lower and upper limit vectors hold element-wise.

We assume that feet s do not slide during ground contacts:

$$\dot{s} = J_s \dot{q}, \tag{4}$$
$$\ddot{s} = J_s \ddot{q} + \dot{J}_s \dot{q} = 0, \tag{5}$$

and that ground contact forces are unilateral, constrained to friction cones of the form [12]:

$$\|f_k^p\| \leq \mu f_k^n \quad \forall f_k \text{ in the ground-feet contact}, \tag{6}$$

where the friction forces f_k^p parallel to the contact surface are limited by the normal force f_k^n with the friction coefficient $\mu > 0$.

B. Hip flexibilities

Flexibility on hip of Talos has been observed to impact meaningfully its control of legs and, therefore, its balance and locomotion [13]. We model this flexibility, as standard [14], by introducing passive joints in the waist-leg connection, where the link cross-section is reduced, as we observe link deflections to concentrate there. The torque on each passive joint is related to its deflection θ as a spring-damper

$$\tau_f = -k_f \theta - d_f \dot{\theta}, \tag{7}$$

with link stiffness k_f and damping d_f coefficients.

As the stiffness is coming for the vertical linkage, we only model the flexibility along pitch and roll deflections, which produce the main impact on foot placement. As a result, our model for the robot Talos has 42 degrees of freedom composed by 32 actuated joints, 4 elastic passive joints and the global position and orientation of the robot.

C. Centroidal dynamics

Balance and locomotion dynamics can be isolated from (1) [15], [16]. Let us consider a Cartesian coordinate system with the origin on the ground surface, assumed to be flat and horizontal, and the axis ^{z} normal to it. So, in the lateral coordinates ^{xy}, this dynamics relates the motion of the Center of Mass (CoM) c of the robot to the Center of Pressure (CoP) p of ground contact forces [17, Chapter 2] as

$$p^{xy} = c^{xy} - \frac{mc^z \ddot{c}^{xy} - S\dot{L}^{xy}}{m(\ddot{c}^z + g^z)} + \frac{\sum_k r_k^z f_k^{xy}}{\sum_k f_k^z}, \tag{8}$$

where g^z is the vertical acceleration due to gravity, m is the total robot mass and $S = \left[\begin{smallmatrix} 0 & -1 \\ 1 & 0 \end{smallmatrix}\right]$ is a $\frac{\pi}{2}$ rotation matrix. Due to unilaterality of ground contact forces (6), the CoP is bound to the support polygon $\mathcal{P}$ [12]:

$$p \in \mathcal{P}(s) \tag{9}$$

that varies depending on the current foot positions s.

III. BALANCE AND LOCOMOTION CONTROL

The general organization of our control scheme is given in Fig. 1. We explain in this section the centroidal stabilizer block, which produces high-frequency feedback based on the centroidal estimated state to follow the reference trajectory produced by the MPC. We explain how this stabilizer is made robust by design.

A. Linear inverted pendulum

In this section, we will rely on a linear model of the centroidal dynamics. Several models have been proposed for legged locomotion, and our method would apply to any of them. Without loss of generality, we then linearize the CoM dynamics as a Linear Inverted Pendulum Model (LIPM)

$$\ddot{c}^{xy} = \omega^2 (c^{xy} - v^{xy}), \tag{10}$$

with some constant value $\omega^2 \approx \frac{g^z}{c^z}$, by introducing the compensated CoP (cCoP) [17], also called virtual repellent point [18] v, which requires us to estimate the bias term

$$n^{xy} \triangleq p^{xy} - v^{xy} \tag{11}$$
$$= \frac{\ddot{c}^{xy}}{\omega^2} - \frac{mc^z \ddot{c}^{xy} - S\dot{L}^{xy}}{m(\ddot{c}^z + g^z)} + \frac{\sum_k r_k^z f_k^{xy}}{\sum_k f_k^z}, \tag{12}$$

based on the previous motion.

Then, we rewrite the dynamics (10) in the discrete form

$$x^+ = Ax + B\dot{v}, \tag{13}$$

without additional approximations, by controlling the rate $\dot{v}$ to be constant on time intervals T [19, Chapter 5.5]. Our chosen state variables and resulting system matrices are:

$$A = \begin{bmatrix} \cosh(\omega T) & \omega^{-1}\sinh(\omega T) & 1 - \cosh(\omega T) \\ \omega \sinh(\omega T) & \cosh(\omega T) & -\omega \sinh(\omega T) \\ 0 & 0 & 1 \end{bmatrix}, \tag{14}$$

$$B = \begin{bmatrix} T - \omega^{-1}\sinh(\omega T) \\ 1 - \cosh(\omega T) \\ T \end{bmatrix}, \qquad x = \begin{bmatrix} c^x & c^y \\ \dot{c}^x & \dot{c}^y \\ v^x & v^y \end{bmatrix} \in \mathcal{X} \tag{15}$$

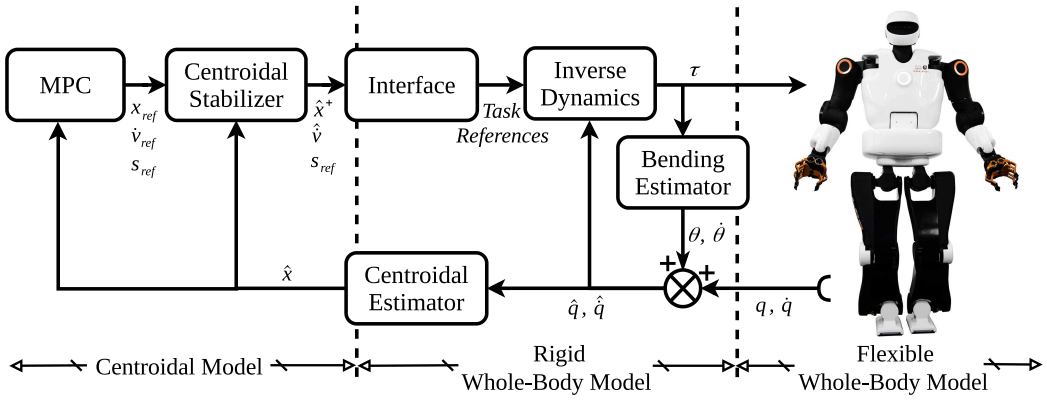

Fig. 1. **Control Diagram:** It is separated in two abstraction levels, the centroidal controller, on the *left*, generates and stabilizes the CoM dynamics, and the whole-body controller, on the *right*, generates the joint torques that must be commanded on the robot actuators.

where ^{x} and ^{y} state variables are decoupled, and admissible states $x \in \mathcal{X}$ satisfy (9): $v^{xy} \in \mathcal{P}(s) - n^{xy}$.

B. Balance controller

As it will be explained in Sec. IV, the MPC produces a reference motion x_{ref}, $\dot{v}_{ref}$, s_{ref} (see Fig. 1), satisfying the dynamics (13)

$$x^+_{ref} = Ax_{ref} + B\dot{v}_{ref}, \tag{16}$$

and the state constraint

$$x_{ref} \in \mathcal{X}_{ref}, \tag{17}$$

We track this reference, based on the estimated state $\hat{x} = x - e_x$, with some error e_x, by commanding the desired next state computed as:

$$\hat{x}^+ = A\hat{x} + B\dot{v}_{ref} + BK(\hat{x} - x_{ref}), \tag{18}$$

with a feedback term $BK(\hat{x} - x_{ref})$ to compensate for errors and disturbances. The resulting real dynamics of the CoM can be obtained by making explicit the estimation errors:

$$x^+ = Ax + B\dot{v}_{ref} + BK(x - x_{ref}) + Be_{\dot{v}} - BKe_x, \tag{19}$$

where $Be_{\dot{v}} = e_{x^+} - Ae_x$ stands for actuation errors and BKe_x for state estimation errors.

These errors deviate the robot from the reference trajectory (16) by some tracking error $\tilde{x} = x - x_{ref}$ as:

$$\tilde{x}^+ = (A + BK)\tilde{x} + B(e_{\dot{v}} - Ke_x). \tag{20}$$

C. Making the controller robust

Provided that $A + BK$ is strictly stable, and disturbances are bounded to some set $\mathcal{D}$

$$e_{\dot{v}} - Ke_x \in \mathcal{D}, \tag{21}$$

we can iterate with the equation (20) to obtain that the tracking error is confined to the minimal Robust Positively Invariant (mRPI) set Ω [20]

$$\tilde{x} = x - x_{ref} \in \Omega \tag{22}$$

of the system, which is convex, compact and contains the origin. This bound, then, guarantees that the state constraint (15) is always satisfied by setting the reference motion such that [21]:

$$x_{ref} \in \mathcal{X}_{ref} \triangleq \mathcal{X} \ominus \Omega. \tag{23}$$

where $\ominus$ represents the Pontryagin difference[1], assuming that $\mathcal{X} \ominus \Omega$ is non-empty. In particular, this constraint restricts the reference cCoP v_{ref} with the safety margin

$$\tilde{v}_{max} = \max_{\tilde{x} \in \Omega} \quad [0\ 0\ 1]\,\tilde{x} \tag{24}$$

that corresponds to the maximum cCoP tracking error [17, Chapter 4.5]. So, we can reduce the motion restrictiveness by choosing a feedback gain K_{opt} that minimizes this tracking error bound:

$$K_{opt} = \underset{K}{\operatorname{argmin}} \quad \tilde{v}_{max}, \tag{25}$$

This problem can be solved, for example with a derivative free solver such as *Nelder-Mead* [22].

IV. PREDICTIVE CONTROL

We consider an MPC scheme to generate on-line the reference motion as described in [23], [5], satisfying the system dynamics (16), state constraint (23) and keeping kinematically feasible step placements $s_{ref} \in \mathcal{S}$ in the stepping area $\mathcal{S}$.

Aiming to simply make the robot walk forward with step lengths close to Δs_{aim}, we set the cost function

$$V = \|\dot{v}_{ref}\|^2 + \|\Delta s_{ref} - \Delta s_{aim}\|^2. \tag{26}$$

In order to maintain stability and recursive feasibility of the planned motion, we restrict the terminal state x^{term}_{ref} to satisfy the capturability condition [24] taking into account the safety margin Ω.

$$c^{term}_{ref} + \frac{\dot{c}^{term}_{ref}}{\omega} \in \mathcal{P}(s^{term}) \ominus \Omega - n^{term}. \tag{27}$$

It has been shown that initializing the MPC computation from the actual robot state x leads to failures easily in our

[1]Given sets A and B, $A \ominus B = \{x | x + B \subseteq A\}$.

current control setting [5]. Instead, the indetermination of the real state (22) must be exploited to let the MPC choose optimally the initial state x_{ref}^{init} satisfying the initial constraint [17, Chapter 6.3.4]:

$$x - x_{ref}^{init} \in \Omega, \tag{28}$$

that ensures the robust exponential stability of the set Ω to the tracking error dynamics (20) [4], and provides some extra freedom in the reference generation. We will show in simulations that it leads to a proper behavior when the robot has to rapidly change its planed motion and stabilize its balance due to a large perturbation.

V. WHOLE-BODY CONTROL

All joint torques are optimally computed using quadratic programming to solve an Inverse Dynamics (ID) problem considering only the actuated degrees of freedom (we use the equivalent configuration $\hat{q} \in \mathbb{R}^{38}$ described in next section) [11]. As standard, the optimization problem is formulated in terms of tasks that define the control goals and constraints [25], [13].

A. Task descriptions

In the *Interface* block, we translate the desired centroidal motion s_{ref}, $\hat{x}^+$, $\hat{\dot{v}} = \dot{v}_{ref} + K(\hat{x} - x_{ref})$ into task references, seeking to avoid conflicts between them in order to reduce the incidence of weight tuning:

Center of Mass: The desired values c^{des}, $\dot{c}^{des}$, $\ddot{c}^{des} \in \mathbb{R}^3$ are obtained from the centroidal state $\hat{x}^+$ and (10).

Feet Motion: Right and left s_R^{des}, $s_L^{des} \in SE(3)$ as well as their time derivatives, are obtained from splines connecting the feet placements s_{ref} [26].

Waist Orientation: The desired orientation $R_w^{des} \in \mathbb{R}^3$, composed by three Euler angles, maintains zero roll and pitch rotations, with the yawl angle as the bisector between right and left feet.

Posture: All joint angles in the robot legs are computed as proposed in [27, Chapter 2.5] to agree with the desired CoM and feet positions. The full desired posture q_j^{des}, $\dot{q}_j^{des}$, $\ddot{q}_j^{des} \in \mathbb{R}^{32}$ is completed with fixed torso and arm references.

Angular Momentum: The desired Angular momentum L^{des}, $\dot{L}^{des} \in R^3$ is obtianed according to the desired configuration $\dot{q}^{des}$, $\ddot{q}^{des} \in \mathbb{R}^{38}$

$$L^{des} = G_{\text{AM}} \dot{q}^{des}, \tag{29}$$

$$\dot{L}^{des} = G_{\text{AM}} \ddot{q}^{des} + \dot{G}_{\text{AM}} \dot{q}^{des}, \tag{30}$$

using the angular part of the centroidal momentum matrix G_{AM}.

Force Distribution: We obtain ground contact wrenches ϕ_R^{des}, $\phi_L^{des} \in \mathbb{R}^6$ from Newton and Euler equations considering the desired values c^{des}, $\ddot{c}^{des}$, $\dot{L}^{des}$. During single support stages the desired centroidal motion determine one unique wrench ϕ^{des}, but during double support stages, we manage the redundancy with quadratic programming by minimizing the wrench magnitude.

B. Policy in task spaces

Joint motion related tasks use forward-kinematic functions $\gamma(q)$ and their time derivatives

$$\dot{\gamma} = \frac{d\gamma}{dq}\dot{q} = J_{task}\dot{q}, \tag{31}$$

$$\ddot{\gamma} = J_{task}\ddot{q} + \dot{J}_{task}\dot{q}, \tag{32}$$

with task-specific Jacobians J_{task}, to approach desired values γ^{des}, $\dot{\gamma}^{des}$, $\ddot{\gamma}^{des}$. Each task can be set as a cost function, for the ID to minimize the square norm

$$V_{task} = \|J_{task}\ddot{q} + \dot{J}_{task}\dot{q} - \pi_{task}\|^2; \tag{33}$$

or as a constraint, for the ID to impose the value

$$J_{task}\ddot{q} + \dot{J}_{task}\dot{q} = \pi_{task}, \tag{34}$$

both using a feedback law π_{task}, with gains K_{P}^{task}, K_{D}^{task}, normally used to produce task consistent accelerations [28]

$$\pi_{task} = K_{\text{P}}^{task}(\gamma - \gamma^{des}) + K_{\text{D}}^{task}(J_{task}\dot{q} - \dot{\gamma}^{des}) + \ddot{\gamma}^{des}. \tag{35}$$

We formulate similarly an angular momentum task as a cost function:

$$V_{\text{AM}} = \|G_{\text{AM}}\ddot{q} + \dot{G}_{\text{AM}}\dot{q} - \pi_{\text{AM}}\|^2, \tag{36}$$

$$\pi_{\text{AM}} = \dot{L}^{des} + K_{\text{P}}^{\text{AM}}(G_{\text{AM}}\dot{q} - L^{des}), \tag{37}$$

using the angular part G_{AM} of the centroidal momentum matrix [29].

Contact force related tasks are formulated to minimize square norms of the form

$$V_{task} = \|D_{task}\phi_k - D_{task}\phi_k^{des}\|^2 \tag{38}$$

for the k-th contact, with an appropriately chosen matrix D_{task}.

VI. COMPENSATION OF DEFLECTIONS

Hip configurations are composed by 3 measured joint rotations $q_{hip} \in \mathbb{R}^3$ and 2 elastic deflections $\theta \in \mathbb{R}^2$, which we approximate based on (7) as:

$$\theta = \frac{\theta_0 - t\,\tau_{hip}}{k\,t + d}, \qquad \dot{\theta} = \frac{\theta - \theta_0}{t}, \tag{39}$$

using the hip roll and pitch commanded torques τ_{hip}, the previous estimated deflections θ_0 and command updating period t.

Let's consider an equivalent hip configuration $\hat{q}_{hip} \in \mathbb{R}^3$ that reproduces the full hip rotation q_{hip}, θ with only 3 actuated joint rotations:

$$R^{zxy}(\hat{q}_{hip}) = R^{yx}(\theta)R^{zxy}(q_{hip}) \tag{40}$$

and equivalent joint velocities

$$\hat{\omega}_{hip} = \omega_\theta + R^{yx}(\theta)\omega_{hip} \tag{41}$$

to obtain the equivalent rate of change on hip joints:

$$\dot{\hat{q}}_{hip} = \left(S^z + R^z(\hat{q}_{hip})S^x + R^{zx}(\hat{q}_{hip})S^y\right)^{-1}\hat{\omega}_{hip}. \tag{42}$$

The rotation matrices $R^{ijk}(\cdot) \in \mathbb{R}^{3\times3}$ show the sequence of rotation axes ^{ijk}, and the selection matrix $S^i \in \mathbb{R}^{3\times3}$ is null except for the i-th component of the diagonal, which is one.

VII. SIMULATIONS AND RESULTS

In the following, we validate our approach in simulations, by evaluating, first, the performance of our stabilizer combined with the compensation of deflections, and then, the environment adaptability provided by the closed-loop MPC. Complete rendering of the whole-body behaviors are available in the compagnion video (which can also be found in HD quality at https://homepages.laas.fr/nvilla/icra22_stal

A. Walking in place

For the first slot of simulations, we consider a precomputed reference motion s_{ref}, x_{ref}, $\dot{v}_{ref}$ for walking in place. Four controller settings are considered and compared. The results are shown in Figures 2 and 3.

Rigid Case: This case is the baseline: the robot is simulated without hip flexibility (nor compensation of deflections) to show the size of tracking errors when no additional disturbances are present. These errors arise mainly from remaining conflicts between the task references described in Section V and numerical errors. While small, these errors still need the stabilizer to be controlled. The resulting motion is plot in Fig. 2 (dotted line) and Fig. 3 (black line).

Uncompensated Case: We simulate the flexible robot, but still without plugging the compensation of deflections. We can observe that the robot goes into strong oscillations that end up with infeasible control actions and see the simulation quickly fails (see light green instable oscillations in Figures 2 and 3.

Compensated Case: By compensating for hip deflections (as explained in Section VI), we obtain a stable simulation, with tracking error sizes that are close to the **Rigid Case** as reported in Fig. 3 (cyan line).

Disturbed Case: As the system constraint allows for much higher tracking errors, we set a more demanding simulation with an external force of 20 N applied at the CoM in ^{y} direction from time 2 s to 7 s, and lateral hits of 200 N in ^{y} direction at time 9 s and 300 N in ^{x} direction at time 13 s. We can observe that the simulation evolves correctly, with admissible tracking errors, as shown in dark green in Figures 2 and 3.

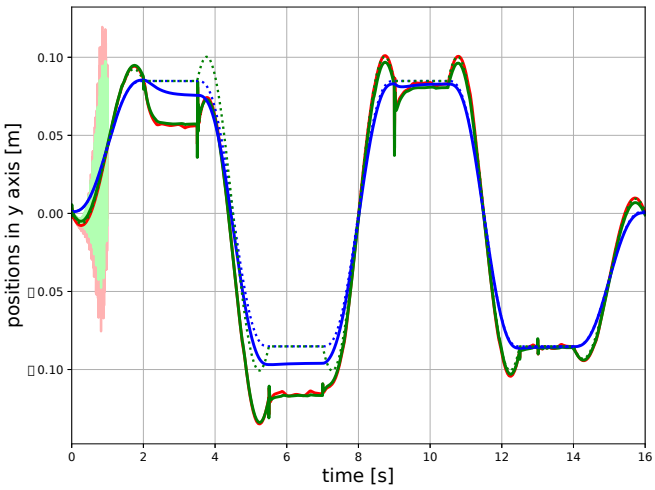

Fig. 2. **Walking in place Simulations:** Time evolution of the CoM *blue*, cCoP *green* and CoP *red*. Reference trajectories are shown with *dotted* lines, and the real values with *solid* lines. The **Uncompensated Case** is shown lighter and the **Disturbed Case** darker. The other cases are almost coincident with the reference lines.

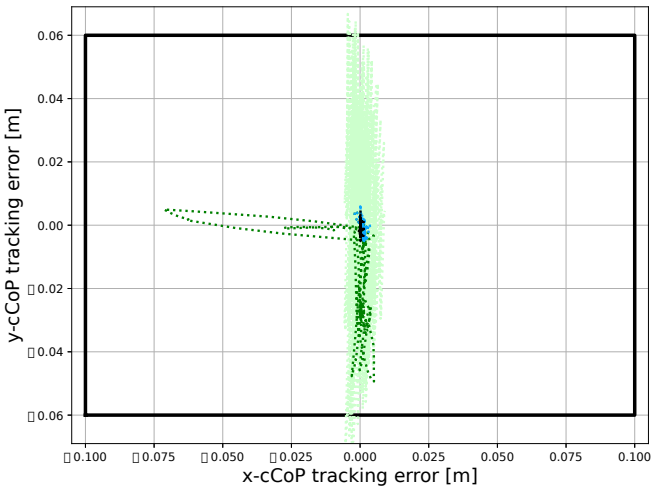

Fig. 3. **Walking in place Simulations:** Single support constraint $\mathcal{P}$ with the tracking error obtained for the **Uncompensated Case** shown in *light green*, the **Disturbed Case** in *dark green*, the **Compensated Case** in *cyan* and the **Rigid Case** in *black*.

B. Push recovery and collision

As a second slot of simulations, we consider two scenarios involving different interactions with the environment. We deploy our MPC scheme aiming to walk forward in both scenarios, working in open-loop and closed-loop to compare their behaviors, which are shown in Figs. 4 and 5.

Lateral Impacts: While walking, the robot is pushed 3 times with 600 N at time 2.7 s, 500 N at 2.9 s and 500 N at 3.1 s. As a result, closed-loop MPC adapts its step placement according to the real state, which allows the robot to maintain a feasible path. On the other hand, the open-loop scheme has no access to the real state, so that gets infeasible at time 3.3 s due to the divergence between real and reference motions. The centroidal trajectory is shown in Fig. 4.

Frontal Collision: During the walk, the robot collides frontally with a solid table that stops the robot when working in closed-loop, or makes it fall backwards up to 5.1 s when working in open-loop. The centroidal trajectory is shown in Fig. 5.

C. Stair climbing

Finally, we simulate the robot in a stair climbing scenario while resisting external forces and hits. The robot is able to keep a stable locomotion even with impacts of up to 300 N. The motion is displayed in the attached video.

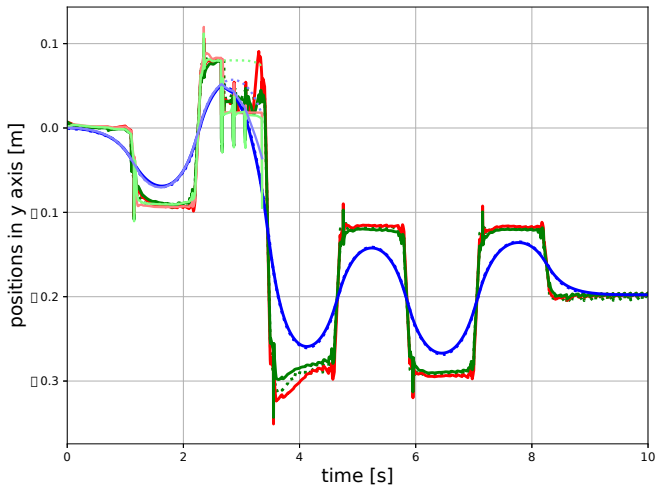

Fig. 4. **Lateral Impacts:** Time evolution of the CoM *blue*, cCoP *green* and CoP *red*. Reference trajectories are shown with *dotted* lines, and the real values with *solid* lines. The open-loop scheme is represented with *lighter* colors and the closed-loop scheme with *darker* colors.

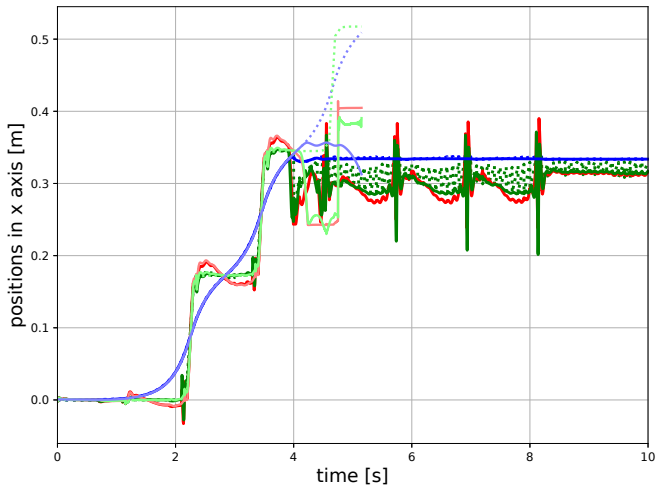

Fig. 5. **Frontal Collision:** Time evolution of the CoM *blue*, cCoP *green* and CoP *red*. Reference trajectories are shown with *dotted* lines, and the real values with *solid* lines. The open-loop scheme is represented with *lighter* colors and the closed-loop scheme with *darker* colors.

VIII. CONCLUSIONS

In this paper, we have proposed a full control scheme to produce a stable and reactive walk on a humanoid robot in spite of modeling errors and other disturbances. The centroidal dynamics is stabilized by state feedback, with gains chosen to minimize the tracking error bound, reducing in this way the restrictiveness introduced for safety in the admissible reference motions (23).

We implemented a closed-loop MPC scheme, based on the mRPI set, to generate the reference motion, taking into account the real state of the robot, under the assumption that disturbances are bounded. This provides a reactive motion replanning, which is extremely useful to operate on unstructured environment. We showed that hip flexibility produce important disturbances on the motion of Talos, and we solved this issue by compensating for hip deflection locally. After this compensation, the remaining disturbances were correctly handled by the centroidal stabilizer.

As a next step, we are currently setting up the experimental evaluation of this control scheme on the real robot Talos.

REFERENCES

[1] D. Kim, J. Di Carlo, B. Katz, G. Bledt, and S. Kim, "Highly dynamic quadruped locomotion via whole-body impulse control and model predictive control," *arXiv preprint arXiv:1909.06586*, 2019.

[2] C. Gehring, P. Fankhauser, L. Isler, R. Diethelm, S. Bachmann, M. Potz, L. Gerstenberg, and M. Hutter, "Anymal in the field: Solving industrial inspection of an offshore hvdc platform with a quadrupedal robot," in *Conference on Field and Service Robotics (FSR)*, 2019.

[3] N. A. Villa, J. Englsberger, and P.-B. Wieber, "Sensitivity of legged balance control to uncertainties and sampling period," *IEEE Robotics and Automation Letters (RA-L)*, vol. 4, no. 4, pp. 3665–3670, 2019.

[4] D. Q. Mayne, M. M. Seron, and S. Raković, "Robust model predictive control of constrained linear systems with bounded disturbances," *Automatica*, vol. 41, no. 2, pp. 219–224, 2005.

[5] N. A. Villa and P.-B. Wieber, "Model predictive control of biped walking with bounded uncertainties," in *IEEE-RAS International Conference on Humanoid Robotics (Humanoids)*, pp. 836–841, 2017.

[6] O. Stasse, T. Flayols, R. Budhiraja, K. Giraud-Esclasse, J. Carpentier, J. Mirabel, A. Del Prete, P. Souères, N. Mansard, F. Lamiraux, *et al.*, "Talos: A new humanoid research platform targeted for industrial applications," in *IEEE-RAS International Conference on Humanoid Robotics (Humanoids)*, pp. 689–695, 2017.

[7] F. Negrello, M. Garabini, M. Catalano, P. Kryczka, W. Choi, D. Caldwell, A. Bicchi, and N. Tsagarakis, "Walk-man humanoid lower body design optimization for enhanced physical performance," in *International Conference on Robotics and Automation (ICRA)*, 2016.

[8] F. Petit, A. Dietrich, and A. Albu-Schäffer, "Generalizing torque control concepts: Using well-established torque control methods on variable stiffness robots," *IEEE Robotics Autom. Mag.*, vol. 22, no. 4, pp. 37–51, 2015.

[9] S. Kajita, K. Yokoi, M. Saigo, and K. Tanie, "Balancing a humanoid robot using backdrive concerned torque control and direct angular momentum feedback," in *ICRA*, 2001.

[10] A. De Luca and W. J. Book, "Robots with flexible elements," in *Springer Handbook of Robotics*, pp. 243–282, Springer, 2016.

[11] G. Nava, F. Romano, F. Nori, and D. Pucci, "Stability analysis and design of momentum-based controllers for humanoid robots," in *IEEE/RSJ International Conference on Intelligent Robots and Systems (IROS)*, pp. 680–687, 2016.

[12] P.-B. Wieber, R. Tedrake, and S. Kuindersma, "Modelling and control of legged robots," in *Springer Handbook of Robotics*, pp. 1203–1234, Springer, 2016.

[13] N. Ramuzat, G. Buondonno, S. Boria, and O. Stasse, "Comparison of position and torque whole-body control schemes on the humanoid robot Talos," in *IEEE International Conference on Advanced Robotics (ICAR)*, 2022.

[14] S. Nakaoka, S. Hattori, F. Kanehiro, S. Kajita, and H. Hirukawa, "Constraint-based dynamics simulator for humanoid robots with shock absorbing mechanisms," in *2007 IEEE/RSJ International Conference on Intelligent Robots and Systems*, pp. 3641–3647, IEEE, 2007.

[15] P.-B. Wieber, "Holonomy and nonholonomy in the dynamics of articulated motion," in *Fast motions in biomechanics and robotics*, pp. 411–425, Springer, 2006.

[16] A. Herzog, N. Rotella, S. Schaal, and L. Righetti, "Trajectory generation for multi-contact momentum control," in *IEEE-RAS International Conference on Humanoid Robots (Humanoids)*, 2015.

[17] N. A. Villa, *Managing uncertainties in legged robots*. PhD thesis, Universite Grenoble Alpes; Inria Grenoble Rhônes-Alpes, 2019.

[18] J. Englsberger, C. Ott, and A. Albu-Schäffer, "Three-dimensional bipedal walking control based on divergent component of motion," *IEEE Transactions on Robotics*, vol. 31, no. 2, pp. 355–368, 2015.

[19] K. Ogata, *Discrete-time control systems*, vol. 8. Prentice-Hall Englewood Cliffs, NJ, 1995.

[20] S. V. Rakovic, E. C. Kerrigan, K. I. Kouramas, and D. Q. Mayne, "Invariant approximations of the minimal robust positively invariant set," *IEEE Transactions on Automatic Control*, vol. 50, no. 3, pp. 406–410, 2005.

[21] D. Q. Mayne, "Control of constrained dynamic systems," *European Journal of Control*, vol. 7, no. 2-3, pp. 87–99, 2001.

[22] F. Gao and L. Han, "Implementing the nelder-mead simplex algorithm with adaptive parameters," *Computational Optimization and Applications*, vol. 51, no. 1, pp. 259–277, 2012.

[23] A. Herdt, H. Diedam, P.-B. Wieber, D. Dimitrov, K. Mombaur, and M. Diehl, "Online walking motion generation with automatic footstep placement," *Advanced Robotics*, vol. 24, no. 5-6, pp. 719–737, 2010.

[24] A. Sherikov, *Balance preservation and task prioritization in whole body motion control of humanoid robots*. PhD thesis, Université Grenoble Alpes, 2016.

[25] A. D. Prete, N. Mansard, O. E. Ramos, O. Stasse, and F. Nori, "Implementing torque control with high-ratio gear boxes and without joint-torque sensors," in *Int. Journal of Humanoid Robotics*, p. 1550044, 2016.

[26] P. Fernbach, *Modèles réduits fiables et efficaces pour la planification et l'optimisation de mouvement des robots à pattes en environnements contraints*. PhD thesis, Université Paul Sabatier-Toulouse III, 2018.

[27] S. Kajita, H. Hirukawa, K. Harada, and K. Yokoi, *Introduction to humanoid robotics*, vol. 101. Springer, 2014.

[28] A. Sherikov, D. Dimitrov, and P.-B. Wieber, "Whole body motion controller with long-term balance constraints," in *IEEE-RAS International Conference on Humanoid Robots (Humanoids)*, pp. 444–450, 2014.

[29] P. M. Wensing and D. E. Orin, "Generation of dynamic humanoid behaviors through task-space control with conic optimization," in *IEEE International Conference on Robotics and Automation*, pp. 3103–3109, 2013.